Final Draft
of the original manuscript:

Angelova, A.; Angelov, B.; Drechsler, M.; Haramus, V.M.; Lesieur, S.:
Protein entrapment in PEGylated lipid nanoparticles
In: International Journal of Pharmaceutics (2013) Elsevier

DOI: 10.1016/j.ijpharm.2013.06.006

Article published in International Journal of Pharmaceutics, 2013, 454, 625–632.
DOI: 10.1016/j.ijpharm.2013.06.006

Protein entrapment in PEGylated lipid nanoparticles

Angelina Angelova[1,2,*], Borislav Angelov[3], Markus Drechsler[4], Vasil M. Garamus[5], and Sylviane Lesieur[1,2]

[1]CNRS UMR8612 Institut Galien Paris-Sud, 5 rue J.B. Clément, F-92296 Châtenay-Malabry cedex, France,

[2]Univ Paris Sud 11, Faculté de Pharmacie, LabEx LERMIT, Châtenay-Malabry, France,

[3]Institute of Macromolecular Chemistry, Academy of Sciences of the Czech Republic, Heyrovsky Sq. 2, CZ-16206 Prague, Czech Republic,

[4]Laboratory for Soft Matter Electron Microscopy, Bayreuth Institute of Macromolecular Research, University of Bayreuth, D-95440 Bayreuth, Germany,

[5]Helmholtz-Zentrum Geesthacht, Centre for Materials and Coastal Research, D-21502 Geesthacht, Germany

*E-mail: Angelina.Angelova@u-psud.fr

Abstract

Defining appropriate delivery strategies of therapeutic proteins, based on lipid nanoparticulate carriers, requires knowledge of the nanoscale organization that determines the loading and release properties of the nanostructured particles. Nanoencapsulation of three cationic proteins (human brain-derived neurotrophic factor (BDNF), α-chymotrypsinogen A, and histone H3) was investigated using anionic nanoparticle (NP) carriers. PEGylated lipid NPs were prepared from self-assembled liquid crystalline phases involving monoolein and eicosapentaenoic acid. Inclusion of the antioxidant α-tocopherol favoured the preparation of stealth hexosome carriers. The purpose of the present work is to reveal the structural features of the protein-loaded lipid nanocarriers by means of high resolution small-angle X-ray scattering (SAXS) and cryogenic transmission electron microscopy (cryo-TEM). The obtained results indicate that protein entrapment is concentration-dependent and may significantly modify the inner liquid crystalline structure of the lipid nanocarriers through changes in the interfacial curvature and hydration.

Keywords: BDNF, neurotrophin, protein nanoencapsulation, hexosomes, PEGylated liquid crystalline nanocarriers.

1. Introduction

Modern methods for protein and peptide drug delivery are based on nanoencapsulation in nanoparticle (NP) carriers (Al-jamal et al., 2011; Azagarsamy et al., 2012; Cortesi et al., 2007; Dai et al., 2006; de Hoog et al., 2012; Géral et al., 2013; Jorgensen et al., 2006; Patton et al., 2005; Plum et al., 2000). Since the emergence of nanomedicine, NP-based delivery strategies have faced various challenges (Allen and Cullis, 2004; Desai, 2012; Dai et al., 2005; Petersen et al., 2012). It has been demonstrated that the physicochemical parameters of lipid-based nanocarriers (size, surface charge, morphology, surface chemistry, stability) may easily be adjusted as to satisfy the requirements for improved drug safety, targeted delivery, appropriate drug release kinetics, and possibility for scaling-up manufacturing (Lim et al., 2012; Martins et al., 2007; Koennings et al, 2007; Carafa et al., 2006; Fujita et al., 1995; Gorodetsky et al., 2004; Guo et al., 2003; Kullberg et al., 2005; Langston et al., 2003; Ramprasad et al., 2003; Ye et al., 2000). Drug delivery applications have shown an essential need of stealth carriers that are stabilized by hydrophilic polymer shells (Freichels, et al., 2011; Keefe et al., 2012; Garcia-Fuentes et al., 2005; Garcia-Santana et al., 2006; Almgren and Rangelov, 2006; Thongborisute et al., 2006). NPs have been surface-modified by polyethyleneglycol (PEG) chains as PEGylation provides reduced immunogenicity and increased circulation time of the vehicles (Arulsudar et al., 2004; Badiee et al., 2007; Chang et al., 2011; Frkanec et al., 2003; Gabizon et al., 1994). Functionalization of the nanocarriers by appropriate ligands (including ligand grafting at the termini of the PEG chains) has favoured targeted protein delivery and has helped avoiding adverse effects (Brgles et al., 2007; Martin et al., 1982; Takeuchi et al., 2003; Torchilin et al., 2001; Visser et al., 2005; Zhang et al., 2005; Wei et al., 2012). Multifunctional lipid-based NPs, involving therapeutic and contrast agents, magnetic components for NP guidance, and/or fluorescence imaging probes, have been developed for theranostic applications (Lesieur et al., 2011; Mulet et al., 2012; Petersen et al., 2012).

Both PEGylated and non-PEGylated liposomes have attracted considerable interest for protein encapsulation (Arifin et al., 2003; Goto et al., 2006, Gregoriadis et al., 1999; Murakami et al., 2006; Rengel et al., 2002; Teiji et al., 2005; Xi et al., 2007; Xu et al., 2012). In such particles, lipid membrane shells isolate the entrapped proteins from the surroundings and serve for efficient protein protection against chemical, physical, or enzymatic degradation (Walde et al., 2001). Furthermore, PEGylation of the NP carriers has contributed to their significantly enhanced bioavailability and minimized side effects (Wang et al., 2012).

Advances in the methods for protein and peptide nanoencapsulation have led to studies of nanostructured lipid particles with multicompartment organizations (Angelov et al., 2012a; Angelova et al., 2005a, 2011, 2012; Géral et al., 2012; Mulet et al., 2012; Nguyen et al., 2011; Puglia, 2008; Woerle et al., 2007; Yaghmur and Glatter, 2009). Inner nanostructures of liquid crystalline types facilitate the encapsulation of large amount of protein molecules in the nanocarriers and may provide protein delivery at enhanced concentration on target sites (Angelov et al., 2003; Angelova et al., 2003; 2005b, 2005c, 2008, 2011; Clogston et al., 2005; Conn et al., 2010; Garti et al., 2012; Misiünas et al., 2012; Negrini and Mezzenga, 2012; Rizwan et al., 2011). Factors controlling the encapsulation and release of biomolecules from liquid crystalline nanocarriers include the type of the inner structural organization, the inner

nanochannel sizes, interface area, surface charge, functionalization, as well as the NP dimensions (Angelov et al., 2013; Angelova et al., 2003, 2012; Chemelli et al., 2012; Negrini and Mezzenga, 2012; Rizwan et al., 2011). Major types of lipid NPs with internal liquid crystalline structures comprise cubosomes, hexosomes, spongosomes, micellar-type cubosomes, multilamellar liposomes, and nanostructured emulsions (Angelov et al., 2006, 2012a, 2012b; Boyd et al., 2006; Conn et al., 2010; Esposito et al., 2005; Dehsorkhi et al., 2011; Géral et al., 2013; Kulkarni et al., 2010; Lai et al., 2010; Mulet et al., 2012; Negrini and Mezzenga, 2012; Phan et al., 2011; Salentinig et al., 2008; Yaghmur and Glatter, 2009). Figure 1 presents examples of lipid NP carriers derived from PEGylated liquid crystalline nanostructures. Such nanocarriers offer unexplored opportunities for protein and peptide drug delivery in view of the suggested link between self-assembled mesophase structure and drug release (Phan et al., 2011).

Figure 1

High resolution electron microscopy and small-angle X-ray scattering (SAXS) studies (Angelov et al., 2007, 2009, 2011a, 2011b; 2012a, 2012b; Cortesi et al., 2007; Woerle et al., 2007; Yaghmur et al., 2007, 2008) have permitted to visualize the single aqueous pore in cubosome nanocarriers, to control the nanochannel sizes in the inner channel networks as well as to detect the earliest stage of the tetrahedral nanochannel formation in cubic lipid particles. It has been suggested that medium- and large-size protein molecules, which are bigger than the aqueous channel diameters, will locate at the interfaces of the nanocubosome subunits, formed inside the cubosome carriers upon protein nanoencapsulation (Angelova et al., 2005c, 2011). The work of Negrini and Mezzenga (2012) has recalled that guest species smaller than the mesophase periodicity will be confined within the aqueous channels and may affect the inner mesophase periodicity, whereas larger species will be expelled and may partition at the grain boundaries of the mesophase domains in the carriers.

The purpose of the present work is to investigate the structural features related to entrapment of different proteins in PEGylated nanocarriers formed by the nonlamellar lipids monoolein and eicosapentaenoic acid (a representative ω-3 polyunsaturated fatty acid). The antioxidant α-tocopherol was included in the lipid mixture in order to induce the formation of an inverted hexagonal (H_{II}) mesophase structure (Boyd et al., 2006). Brain-derived neurotrophic factor (BDNF), α-chymotrypsinogen A, and histone H3 are considered as examples. All three proteins are basic proteins, i.e. are positively charged at pH < pI (see Table 1). BDNF and α-chymotrypsinogen A are soluble in aqueous medium and do not aggregate under the investigated solution conditions. At variance, histone, which is characterized essentially by α–helical content (Arents et al., 1991), is less soluble and was studied as a model of protein aggregation at elevated concentrations. The α–tocopherol component (promoting the hexosome carrier formation) was not studied in the case of histone H3 encapsulation taking into account the geometrical constraints for entrapment of large protein aggregates inside the fine channels of the hexosome particles. The resulting nanoscale organizations were revealed by cryogenic transmission electron microscopy (cryo-TEM) and X-ray structural analysis (SAXS) in order to evaluate the ability of the investigated PEGylated lipid NPs for protein upload.

2. Materials and Methods

2.1. Materials and samples preparation

Monoolein (MO) (1-monooleoyl-rac-glycerol, C18:1c9, MW 356.54, powder, purity >99.5%), *cis*-5,8,11,14,17 eicosapentaenoic acid (EPA) (20:5, MW 302.45, oil phase, analytical standard, purity ≥98.5%), α-tocopherol (Vit E) (MW 430.71, Ph Eur grade), D-α-tocopherol polyethyleneglycol 1000 succinate (V_{1000}) (MW 1531, waxy solid, CMC ~ 0.02% by weight) were purchased from Sigma-Aldrich-Fluka (Saint-Quentin, France). The PEGylated lipid 1,2-dioleyl-*sn*-glycero-3-phosphoethanolamine-N-[methoxy (polyethylene glycol)-2000] (DOPE-PEG_{2000}) (MW 2801.51, powder, purity >99.5%, CMC ~ 2×10^{-5} M) was a product of Avanti Polar Lipids (COGER, France). Carrier-free human recombinant brain-derived neurotrophic factor (hrBDNF, MW 13.6 kDa) was purchased from R&D Systems. The proteins α-chymotrypsinogen A (type II from bovine pancreas, purified by 6×crystallization, salt-free, lyophilized powder, MW 25.656 kDa) and histone H3 (type III-S lysine-rich fraction, from calf thymus, MW 15.3 kDa) were products of Sigma (Saint-Quentin, France). Phosphate buffer solution ($1x10^{-2}$ M, pH 7) was prepared using the inorganic salts NaH_2PO_4 and Na_2HPO_4 (p.a. grade, Fluka, Saint-Quentin) and MilliQ water of resistivity 18.2 MΩ.cm (Millipore Co., Molsheim).

Liquid crystalline lipid NP formulations were prepared by the method of hydration of a dry lipid film followed by physical agitation (Angelov et al., 2011b). The organic solvent (chloroform) was evaporated under flow of nitrogen gas and the resulting lipid mixtures were lyophilized overnight. Towards mesophase formation, lipid assemblies were initially incubated with aqueous buffer during 30 min followed by repeated vortexing. Subsequently, 15 min agitation was performed in ice medium using a sonication bath with a moderate frequency (40 kHz, Branson 2510) (Branson Ultrasonics, Geneve). The PEGylated amphiphiles (DOPE-PEG_{2000} and V_{1000}) served as solubilizing and dispersing agents for the MO/EPA/VitE liquid crystalline phases. The resulting NP formulations were incubated with proteins for several hours, homogenized, and studied by means of SAXS, cryo-TEM, and QELS.

2.2. Small-angle X-ray scattering (SAXS)

SAXS experiments were performed at the P12 BioSAXS beamline of the European Molecular Biology Laboratory (EMBL) at the storage ring PETRA III of the Deutsche Elektronen Synchrotron (DESY, Hamburg, Germany) at 20 °C using a Pilatus 2M detector (1475 x 1679 pixels) (Dectris, Switzerland) and synchrotron radiation with a wavelength λ = 1 Å. The sample-to-detector distance was 3 m. The q-vector was defined as $q = (4\pi/\lambda) \sin \theta$, where 2θ is the scattering angle. The q-range was calibrated using the diffraction patterns of silver behenate. The experimental data were normalized with respect to the incident beam intensity. The background scattering of the solvent buffer was subtracted. The solvent scattering was measured before and after every lipid NP or protein-containing sample in order to control for eventual sample-holder contamination. Eight consecutive frames comprising measurements for the solvent, the sample, and the solvent were acquired. No measurable radiation damage was detected by the comparison of eight successive time frames with 5 s exposures. The final scattering curve was obtained using the program PRIMUS by averaging the scattering data

collected from the measured frames. An automatic sample changer adjusted for sample volume of 15 μL and a filling cycle of 20 s was used.

2.3. Cryogenic transmission electron microscopy (Cryo-TEM)

For cryo-TEM studies, a sample droplet of 2 µL was put on a lacey carbon film covered copper grid (Science Services, Munich, Germany), which was hydrophilized by glow discharge for 15 s. Most of the liquid was then removed with blotting paper, leaving a thin film stretched over the lace holes. The specimens were instantly shock frozen by rapid immersion into liquid ethane and cooled to approximately 90 K by liquid nitrogen in a temperature-controlled freezing unit (Zeiss Cryobox, Zeiss NTS GmbH, Oberkochen, Germany). The temperature was monitored and kept constant in the chamber during all the sample preparation steps. After the specimens were frozen, the remaining ethane was removed using blotting paper. The specimen was inserted into a cryo transfer holder (CT3500, Gatan, Munich, Germany) and transferred to a Zeiss EM922 Omega energy-filtered TEM (EFTEM) instrument (Zeiss NTS GmbH, Oberkochen, Germany). Examinations were carried out at temperatures around 90 K. The TEM instrument was operated at an acceleration voltage of 200 kV. Zero-loss-filtered images ($\Delta E = 0$ eV) were taken under reduced dose conditions (100-1000 e/nm^2). All images were recorded digitally by a bottom-mounted charge-coupled device (CCD) camera system (Ultra Scan 1000, Gatan, Munich, Germany) and combined and processed with a digital imaging processing system (Digital Micrograph GMS 1.8, Gatan, Munich, Germany). All images were taken very close to focus or slightly under the focus (some nanometers) due to the contrast enhancing capabilities of the in-column filter of the used Zeiss EM922 Omega. In EFTEMs, deep underfocussed images can be totally avoided.

2.4. Quasi-elastic light scattering (QELS)

Particle size distributions in the investigated dispersed lipid samples were determined using a Nanosizer apparatus (Nano-ZS90, MALVERN, Orsay) equipped with a Helium-Neon laser of 633 nm wavelength. The samples were diluted to 1 mM lipid concentration prior to measurement in 1 cm thick cells and analyzed in an automatic mode using the following experimental parameters: temperature 25 ^{o}C; scattering angle, 90°; refracting index, 1.33; environment medium viscosity, 0.890 cP. The average hydrodynamic diameter, d_h, was calculated considering the mean translational diffusion coefficient, D, of the particles in accordance with the Stokes-Einstein law for spherical particles in the absence of interactions: $d_h = k_B T/3\eta\pi D$, where k_B is the Boltzmann constant, T is temperature, and η is the viscosity of the aqueous medium. Three measurements with the same cell were averaged for every sample. The protein solutions were investigated at chosen concentrations (Table 1). The results were analyzed using the MALVERN Zetasizer software (version 6.11).

3. Results and discussion

Sterically stabilized lipid nanocarriers were prepared by hydration of mixed lipid films consisting of self-assembled MO/EPA/VitE or MO/EPA mixtures and functionalized by the PEGylated amphiphiles DOPE-PEG_{2000} or V_{1000}. Monoolein (MO) and α-tocopherol (VitE) are neutral lipids of nonlamellar propensities, whereas eicosapentaenoic acid (EPA) is a ω-3 polyunsaturated anionic lipid. The role of α-tocopherol (VitE) is to increase the interfacial curvature of the cubic-phase forming lipid monoolein as well as to induce the formation of inverted hexagonal phase structures. The latter may provide sustained release of entrapped proteins from nanochanneled-type carriers. The investigated PEGylated amphiphiles form PEGylated micelles in individual assemblies at concentrations above their critical micellar concentrations (CMC). The molar percentages of these PEGylated components, included in the studied liquid crystalline lipid structures, were optimized in a manner ensuring only a partial shield of the charges of the lipid NPs, which facilitate the protein entrapment through electrostatic interactions. In the following, we present the structural results obtained for lipid NPs (MO/EPA/VitE/V_{1000} or MO/EPA/DOPE-PEG_{2000}) interacting with the proteins BDNF, α-chymotrypsinogen A, or histone H3. Taking into account the possible aggregation of histone, the latter was not selected for studies with the H_{II} phase carriers. The associated form of histone would have a minor chance for loading into the nanochannels of hexosome carriers formed by the self-assembled MO/EPA/VitE/V_{1000} (71/17/8/4 mol.%) mixture.

3.1. Human recombinant brain-derived neurotrophic factor (BDNF)

Small-angle X-ray scattering (SAXS) patterns of PEGylated lipid NPs studied for nanoencapsulation of the neurotrophin BDNF are shown in Figure 2a. The SAXS curve presented in the inset characterizes the NPs structure (MO/EPA/VitE/V_{1000}, 71/17/8/4 mol.%) formed before the addition of the therapeutic protein. BDNF exerts its neuroprotective bioactivity at concentrations in the nanogram range. Therefore, the nanoencapsulation studies should take into account that BDNF can cause adverse effects in a concentrated state. For this reason and because of its high cost, the interaction of recombinant human BDNF with lipid NPs was studied at a chosen relatively low protein concentration of 8 μg/ml. Under these conditions, BDNF was completely soluble in the aqueous medium (Table 1). The positively charged protein was allowed to interact with the nanocarriers involving the anionic lipid EPA.

The analysis of the obtained SAXS patterns established that both blank (MO/EPA/VitE/V_{1000}) and protein-loaded lipid NPs have inner mesophase structures of an inverted hexagonal (H_{II}) type (Fig. 2a). The formation of stable PEGylated hexosomes in the lipid formulations was favoured by the hydrophobic component VitE, which essentially increases the lipid monolayer curvature and augments the nonlamellar propensity of the mixture. In addition, VitE provides an antioxidant functionality of the carriers, which is of interest for their therapeutic applications. The included higher percentage of VitE (8 mol%) with regard to the PEGylated component V_{1000} (4 mol.%) contributes to compensate the decrease of the monolayer curvature, due to the PEGylation, and to induce a nonlamellar supramolecular

organization of hexagonally-packed aqueous channels (Fig. 1a). The resolved Bragg peaks, spaced in the ratio 1: √3: √4: √7, determine an inner H_{II}-lattice periodicity of 6.53 nm. The water channel diameter, D_W, was calculated using a literature method (Turner and Gruner, 1992). The protein hydrodynamic size, d_h, was determined by quasi-elastic light scattering (QELS) (see Table 1). The obtained results indicate that the aqueous channels in the hexosome nanocarriers are sufficiently large (D_W = 3.42 nm) to accommodate the soluble protein BDNF (d_h = 2.3 nm).

Figure 2

Both the SAXS (Fig. 2a) and the cryo-TEM (Fig. 2b) results confirmed that BDNF does not modify the structural periodicity of the lipid nanocarriers at the investigated protein concentration. Figure 2b shows the characteristic morphology of the hexosome NPs. The inset presents the Fast Fourier transform (FFT) derived from the cryo-TEM image. It reveals the inverted hexagonal (H_{II}) mesophase periodicity corresponding to an ordered structure of aqueous nanochannels available for BDNF loading. The hexosome particles in the MO/EPA/VitE/V_{1000} (71/17/8/4 mol.%) formulation displayed mean hydrodynamic diameters of ~400 nm in QELS measurements. This is in agreement with the electron microscopy results. A coexisting fraction of small vesicles (d_h = 38 nm) was also observed in the cryo-TEM and QELS studies as a result of nonequilibrium effects related to the dispersion of the nanoparticulate system under energy input.

3.2. α-Chymotrypsinogen A

The NP carriers studied above (MO/EPA/VitE/V_{1000}, 71/17/8/4 mol.%) were allowed to interact also with the positively charged enzyme α-chymotrypsinogen A of concentration 4 mg/mL. The obtained results revealed that the protein, displaying surface activity under these conditions, affected the curvature of the lipid assembly. The SAXS patterns (Fig. 3a) and the cryo-TEM images (Fig. 3b) clearly demonstrate that the performed nanoencapsulation resulted in a structural change of the H_{II}-phase lipid nanocarriers (MO/EPA/VitE/V_{1000}, 71/17/8/4 mol.%) (Fig. 3a, inset) toward protein-loaded NPs with new structural and morphological features. The SAXS pattern of the protein-containing NPs (Fig. 3a) corresponds to the form factor of the NP scattering rather than to Bragg diffraction peaks of an inner periodic structure. The blue bars (which mark the positions of the H_{II}-phase peaks of the blank NPs) show that the Bragg peaks are vanished in the presence of α-chymotrypsinogen A as a result of the hexosome NP transformation into another type of NPs.

Figure 3

Indeed, the cryo-TEM image (Fig. 3b) shows double vesicular structures in the protein-loaded lipid NP formulation. The mean hydrodynamic diameter of the α-chymotrypsinogenA-loaded particles determined by QELS (d_h = 458 nm) is slightly different from that of the blank

hexosome carriers (d_h ~ 400 nm). Coexisting bilamellar lipid NPs (d_h ~ 80 nm) were also observed (Fig. 3b, inset). They are likely obtained upon the membrane fragmentation (from larger to smaller particles), which is provoked by the surface-active protein. The darker interior of the bilamellar vesicles is due to thickness variation (the transmission is reduced because the electrons must pass through extra bilayers). No evidence for protein aggregation is obtained at the studied concentration.

3.3. Histone

PEGylated lipid NPs (MO/EPA/DOPE-PEG_{2000} (69/28/3 mol.%) were incubated with histone H3, which is a basic protein of prevailing α-helical content. The employed lipid mixture did not display a propensity for hexosome formation similarly to the recently reported NPs involving DOPE-PEG_{2000} (Angelov et al., 2012b). The mean particle size in the blank NP formulation (MO/EPA/DOPE-PEG_{2000}, 69/28/3 mol.%), determined by QELS, was d_h = 142 nm and was attributed to coexisting small cubosomes and vesicles (see the histogram in Figure 4b). The solution scattering of histone is presented in Fig. 4a together with the derived pair distance distribution function $\rho(r)$ (inset). The size of the histone octamer, estimated from these SAXS results, is 4.5 nm. The QELS data (Fig. 4a, red histogram) showed that the histone units (4.5 nm) begin to associate into aggregates at the studied solution concentration. The hydrodynamic particle diameter of the associated protein was d_h = 255 nm at concentration of 4 mg/ml (Fig. 4a, inset).

Figure 4

Figure 5a (inset) shows the NP scattering of the blank MO/EPA/DOPE-PEG_{2000} (69/28/3 mol.%) carriers. The observed SAXS is typical for a mixture of membrane-type lipid nanocarriers. Attempts to load these small cubosomes and vesicles with histone (4 mg/ml) did not permit significant entrapment of the protein inside the NPs, because of its associated state in solution. The SAXS pattern of the particles incubated with protein is shown in Fig. 5a. The performed QELS investigation also confirmed the aggregation of histone in lipid NP formulations (Fig. 4b, right panel). The particle size distributions in a blank lipid NP formulation and in a protein-containing lipid (MO/EPA/DOPE-PEG_{2000}, 69/28/3 mol.%) formulation determined mean NP diameters of d_h = 142 nm and 220 nm, respectively.

Figure 5

The obtained cryo-TEM image (Figure 5b) shows a noticeable phase separation of the protein from the lipid NPs (MO/EPA/DOPE-PEG_{2000}, 69/28/3 mol.%). The difficulty to entrap histone, associated in aggregates, into such small PEGylated NP carriers implies that larger lipid particles or even bulk liquid crystalline phases would be more appropriate for confinement and encapsulation of this hydrophobic α-helical protein. At variance, BDNF and α-chymotrypsinogen A appeared to be homogeneously distributed in the investigated NP

systems and can be entrapped both in hexosome and vesicular carriers of similar lipid compositions.

4. Conclusion

Further to the recently reported protein-containing PEGylated cubosomes (Angelov et al., 2012a), the present study of nanostructured liquid crystalline lipid NPs demonstrates that the interaction of PEGylated hexosomes with cationic protein molecules may lead to either preservation or dramatic changes in the inner structure of the NPs. The obtained results revealed that the entrapped protein, depending on its concentration and amphiphilicity, may influence the curvature of the lipid assemblies and even transform the internal nanostructure of channels into a different structural organization. Efficient protein encapsulation was achieved for recombinant BDNF and α-chymotrypsinogen A. Histone in its aggregated state showed a tendency to phase separate from the lipid NP carriers at the investigated protein concentration. The outcome of this structural study confirms that SAXS, QELS and cryo-TEM measurements are very powerful methods in the design of protein drug delivery carriers and should be recommended as tools of ultimate pharmaceutical relevance permitting to control the protein nanoencapsulation process.

Acknowledgements

A.A. and S.L. acknowledge the supports from the programmes ANR SIMI10 Nanosciences and LabEx LERMIT (Laboratoire d'excellence de Recherche sur le Médicament et l'Innovation Thérapeutique). B.A. acknowledges the Czech Science Foundation Grant No. P208/10/1600 and the help of Dr. Manfred Roessle (EMBL) during the SAXS experiments. M.D. acknowledges the support from BIMF (Bayreuth Institute of Macromolecular Research) and BZKG (Bayreuth Center for Colloids and Interfaces).

References

Allen, T.M., Cullis, P.R., 2004. Drug delivery systems: entering the mainstream. Science 303, 1818-1822.

Al-jamal, W.T., Kostarelos, K., 2011. Liposomes: from a clinically established drug delivery system to a nanoparticle platform for theranostic nanomedicine. Acc. Chem. Res. 44, 1094–1104.

Almgren, M., Rangelov, S., 2006. Polymorph dispersed particles from the bicontinuous cubic phase of glycerol monooleate stabilized by PEG-copolymers with lipid-mimetic hydrophobic anchors. J. Dispersion Sci. Technol. 27, 599−609.

Angelov, B., Angelova, A., Ollivon, M., Bourgaux, C., Capitelli, A., 2003. Diamond-type lipid cubic phase with large water channels. J. Am. Chem. Soc. 125, 7188-7189.

Angelov, B., Angelova, A., Papahadjopoulos-Sternberg, B., Lesieur, S., Sadoc, J.-F., Ollivon, M., Couvreur, P., 2006. Detailed structure of diamond-type lipid cubic nanoparticles. J. Am. Chem. Soc. 128, 5813-5817.

Angelov, B., Angelova, A., Garamus, V.M., Le Bas, G., Lesieur, S., Ollivon, M., Funari, S.S., Willumeit, R., Couvreur, P., 2007. Small-angle neutron and X-ray scattering from amphiphilic stimuli-responsive diamond-type bicontinuous cubic phase. J. Am. Chem. Soc. 129, 13474−13479.

Angelov, B., Angelova, A., Vainio, U., Garamus, V. M., Lesieur, S., Willumeit, R., Couvreur, P., 2009. Long living intermediates during a lamellar to a diamond-cubic lipid phase transition: a SAXS investigation. Langmuir 25, 3734-3742.

Angelov, B., Angelova, A., Mutafchieva, R., Lesieur, S., Vainio, U., Garamus, V.M., Jensen, G.V., Pedersen, J.S., 2011a. SAXS investigation of a cubic to a sponge (L_3) phase transition in self-assembled lipid nanocarriers. Phys. Chem. Chem. Phys. 13, 3073-3081.

Angelov, B., Angelova, A., Filippov, S., Karlsson, G., Terrill, N., Lesieur, S., Štěpánek, P., 2011b. Topology and internal structure of PEGylated lipid nanocarriers for neuronal transfection: synchrotron radiation SAXS and cryo-TEM studies. Soft Matter 7, 9714–9720.

Angelov, B., Angelova, A., Papahadjopoulos-Sternberg, B., Hoffmann, S.V., Nicolas, V., Lesieur, S., 2012a. Protein-containing PEGylated cubosomic particles: freeze-fracture electron microscopy and synchrotron radiation circular dichroism study. J. Phys. Chem. B 116, 7676-7686.

Angelov, B., Angelova, A., Garamus, V.M., Drechsler, M., Willumeit, R., Mutafchieva, R., Štěpánek, P., Lesieur, S., 2012b. Earliest stage of the tetrahedral nanochannel formation in cubosome particles from unilamellar nanovesicles. Langmuir 28, 16647−16655.

Angelov, B., Angelova, A., Filippov, S., Narayanan, T., Drechsler, M., Štěpánek, P., Couvreur, P.; Lesieur, S., 2013. DNA/fusogenic lipid nanocarrier assembly: millisecond structural dynamics. *J. Phys. Chem. Lett. 4*, 1959–1964.

Angelova, A., Ollivon, M., Campitelli, A., Bourgaux, C., 2003. Lipid cubic phases as stable nanochannel network structures for protein biochip development: X-ray diffraction study. Langmuir 19, 6928-6935.

Angelova, A., Angelov, B., Papahadjopoulos-Sternberg, B., Bourgaux, C., Couvreur, P., 2005a. Protein driven patterning of self-assembled cubosomic nanostructures: long oriented nanoridges. J. Phys. Chem. B 109, 3089-3093.

Angelova, A., Angelov, B., Papahadjopoulos-Sternberg, B., Ollivon, M., Bourgaux, C., 2005b. Structural organisation of proteocubosome carriers involving medium- and large-size proteins. J. Drug Deliv. Sci. Tech. 15, 108-112.

Angelova, A., Angelov, B., Papahadjopoulos-Sternberg, B., Ollivon, M., Bourgaux, C., 2005c. Proteocubosomes: nanoporous vehicles with tertiary organized fluid interfaces. Langmuir 21, 4138-4143.

Angelova, A., Angelov, B., Lesieur, S., Mutafchieva, R., Ollivon, M., Bourgaux, C., Willumeit, R., Couvreur, P., 2008. Dynamic control of nanofluidic channels in protein drug delivery vehicles. J. Drug Deliv. Sci. Tech. 18, 41-45.

Angelova, A., Angelov, B., Mutafchieva, R., Lesieur, S., Couvreur, P., 2011. Self-assembled multicompartment liquid crystalline lipid carriers for protein, peptide, and nucleic acid drug delivery. Acc. Chem. Res. 44, 147−156.

Angelova, A., Angelov, B., Garamus, V.M., Couvreur, P., Lesieur, S., 2012. Small-angle X-ray scattering investigations of biomolecular confinement, loading, and release from liquid crystalline nanochannel assemblies. J. Phys. Chem. Lett. 3, 445-457.

Arents, G., Burlingame, R. W., Wang, B. C., Love, W. E., Moudrianakis, E. N. 1991. The nucleosomal core histone octamer at 3.1 Å resolution: a tripartite protein assembly and a left-handed superhelix. Proc. Natl. Acad. Sci. USA 88, 10148–52.

Arifin, D.R., Palmer, A.F., 2003. Determination of size distribution and encapsulation efficiency of liposome-encapsulated hemoglobin blood substitutes using asymmetric flow field-flow fractionation coupled with multi-angle static light scattering. Biotechnol. Prog. 19, 1798-1811.

Arulsudar, N., Subramanian, N., Mishra, P., Chuttani, K., Sharma, R.K., Murthy, R.S.R., 2004. Preparation, characterization, and biodistribution study of technetium-99m-labeled leuprolide acetate-loaded liposomes in Ehrlich ascites tumor-bearing mice. AAPS J. Pharm. Sci. 6, 45-56.

Azagarsamy, M.A., Alge, D.L., Radhakrishnan, S.J., Tibbitt, M.W., Anseth, K.S., 2012. Photocontrolled nanoparticles for on-demand release of proteins. Biomacromolecules 13, 2219-2224.

Badiee, A., Jaafari, M.R., Khamesipour, A., 2007. Leishmania major: Immune response in BALB/c mice immunized with stress-inducible protein 1 encapsulated in liposomes. Exp. Parasitol. 115, 127-134.

Boyd, B. J., Whittaker, D. V., Khoo, S.-M., Davey, G., 2006. Hexosomes formed from glycerate surfactant - formulation as a colloidal carrier for irinotecan. Int. J. Pharm. 318, 154−162.

Brgles, M., Mirosavljevic, K., Noethig-Laslo, V., Frkanec, R., Tomasic, J., 2007. Spin-labelling study of interactions of ovalbumin with multilamellar liposomes and specific anti-ovalbumin antibodies. Int. J. Biol. Macromol. 40, 312-318.

Carafa, M., Marianecci, C., Annibaldi, V., Di Stefano, A., Sozio, P., Santucci, E., 2006. Novel O-palmitoylscleroglucan-coated liposomes as drug carriers: development, characterization and interaction with leuprolide. Int. J. Pharm. 325, 155-162.

Chang, W.K., Tai, Y.J., Chiang, C.H., Hu, C.S., Hong, P.D., Yeh, M.K., 2011. The comparison of protein-entrapped liposomes and lipoparticles: preparation, characterization, and efficacy of cellular uptake. Int. J. Nanomed. 6, 2403-2417.

Chemelli, A., Maurer, M., Geier, R., Glatter, G., 2012**.** Optimized loading and sustained release of hydrophilic proteins from internally nanostructured particles. Langmuir 28, 16788–16797.

Clogston, J., Caffrey, M., 2005. Controlling release from the lipidic cubic phase. amino acids, peptides, proteins and nucleic acids. J. Control. Release 107, 97−111.

Conn, C.E., Darmanin, C., Sagnella, S.M., Mulet, X., Greaves, T.L., Varghese, J.N., Drummond, C.J., 2010. Incorporation of the dopamine D2L receptor and bacteriorhodopsin within bicontinuous cubic lipid phases. 1. Relevance to in meso crystallization of integral membrane proteins in monoolein systems. Soft Matter 6, 4828–4837.

Cortesi, R., Esposito, E., Corradini, F., Sivieri, E., Drechsler, M., Rossi, A., Scatturin, A., Menegatti, E. 2007. Non-phospholipid vesicles as carriers for peptides and proteins: production, characterization and stability studies. Int. J. Pharm. 339, 52–60.

Dai, C.Y., Wang, B.C., Zhao, H.W., Li, B., 2005. Factors affecting protein release from microcapsule prepared by liposome in alginate. Colloid Surf. B-Biointerfaces 42, 253-258.

Dai, C.Y., Wang, B.C., Zhao, H.W., Li, B., Wang, H., 2006. Preparation and characterization of liposomes-in-alginate (LIA) for protein delivery system. Colloid Surf. B-Biointerfaces 47, 205-210.

de Hoog, H.-P.M., Nallani, M., Tomczak, N., 2012. Self-assembled architectures with multiple aqueous compartments. Soft Matter 8, 4552–4561.

Dehsorkhi, A., Castelletto, V., Hamley, I.W., Harris, P.J.F., 2011. Multiple hydrogen bonds induce formation of nanoparticles with internal microemulsion structure by an amphiphilic copolymer. Soft Matter 7, 10116–10121.

Desai, N., 2012. Challenges in development of nanoparticle-based therapeutics. AAPS Journal 14, 282-295.

Esposito, E., Cortesi, R., Drechsler, M., Paccamiccio, L., Mariani, P., Contado, C., Stellin, E., Menegatti, E., Bonina, F., Puglia, C., 2005. Cubosome dispersions as delivery systems for percutaneous administration of indomethacin. Pharm. Res. 22, 2163−2173.

Freichels, H., Jerome, R., Jerome, C., 2011. Sugar-labeled and PEGylated (bio)degradable polymers intended for targeted drug delivery systems. Carbohydrate Polym. 86, 1093-1106.

Frkanec, R., Noethig-Laslo, V., Vranesic, B., Mirosavljevic, K., Tomasic, J., 2003. A spin labelling study of immunomodulating peptidoglycan monomer and adamantyltripeptides entrapped into liposomes. Biochim. Biophys. Acta-Biomembr. 1611, 187-196.

Fujita, H., Sasaki, R., Yoshikawa, M., 1995. Potentiation of the antihypertensive activity of orally administered ovokinin, a vasorelaxing peptide derived from ovalbumin, by emulsification in egg phosphatidylcholine. Biosci. Biotechnol. Biochem. 59, 2344-2345.

Gabizon, A., Catane, R., Uziely, B., Kaufman, B., Safra, T., Cohen, R., Martin, F., Huang, A., Barenholz, Y., 1994. Prolonged circulation time and enhanced accumulation in malignant exudates of doxorubicin encapsulated in polyethylene-glycol coated liposomes. Cancer Res. 54, 987-992.

Garcia-Fuentes, M., Torres, D., Alonso, M.J., 2005. New surface-modified lipid nanoparticles as delivery vehicles for salmon calcitonin. Int. J. Pharm. 296, 122-132.

Garcia-Santana, M.A., Duconge, J., Sarmiento, M.E., Lanio-Ruiz, M.E., Becquer, M.A., Izquierdo, L., Acosta-Dominguez, A., 2006. Biodistribution of liposome-entrapped human gamma-globulin. Biopharm. Drug Dispos. 27, 275-283.

Garti, N., Somasundaran, P., Mezzenga, R. (Eds.), 2012. Self-assembled supramolecular architectures: Lyotropic liquid crystals, 1st ed., John Wiley & Sons, Inc., Hoboken, NJ.

Géral, C., Angelova, A., Angelov, B., Nicolas, V., Lesieur, S., 2012. Chapter 11: Multicompartment lipid nanocarriers for targeting of cells expressing brain receptors, in: Garti, N., Somasundaran, P., Mezzenga, R. (Eds.), Self-assembled supramolecular architectures: Lyotropic liquid crystals. John Wiley & Sons, Inc., New Jersey, pp. 319-355.

Géral, C., Angelova, A., Lesieur, S., 2013. From molecular to nanotechnology strategies for delivery of neurotrophins: emphasis on brain-derived neurotrophic factor (BDNF). Pharmaceutics 5, 127-167.

Gorodetsky, R., Levdansky, L., Vexler, A., Shimeliovich, I., Kassis, I., Ben-Moshe, M., Magdassi, S., Marx, G., 2004. Liposome transduction into cells enhanced by haptotactic peptides (haptides) homologous to fibrinogen C-termini. J. Control. Release 95, 477-488.

Goto, T., Morishita, M., Nishimura, K., Nakanishi, M., Kato, A., Ehara, J., Takayama, K., 2006. Novel mucosal insulin delivery systems based on fusogenic liposomes. Pharm, Res. 23, 384-391.

Gregoriadis, G., McCormack, B., Obrenovic, M., Saffie, R., Zadi, B., Perrie, Y., 1999. Vaccine entrapment in liposomes. Methods 19, 156-162.

Guo, J., Ping, Q., Jiang, G., Huang, L., Tong, Y., 2003. Chitosan-coated liposomes: characterization and interaction with leuprolide. Int. J. Pharm. 260, 167-173.

Jorgensen, L., Moeller, E.H., Van D.W.M., Nielsen, H.M., Frokjaer, S., 2006. Preparing and evaluating delivery systems for proteins. Eur. J. Pharm. Sci. 29, 174-182.

Keefe, A.J., Jiang, S., 2012. Poly(zwitterionic)protein conjugates offer increased stability without sacrificing binding affinity or bioactivity. Nature Chem. 4, 59-63.

Koennings, S., Sapin, A., Blunk, T., Menei, P., Goepferich, A., 2007. Towards controlled release of BDNF - manufacturing strategies for protein-loaded lipid implants and biocompatibility evaluation in the brain. J. Control. Release 119, 163–172.

Kulkarni, C.V., Mezzenga, R., Glatter, O., 2010. Water-in-oil nanostructured emulsions: towards the structural hierarchy of liquid crystalline materials. Soft Matter 6, 5615−5624.

Kullberg, E.B., Wei, Q.C., Capala, J., Giusti, V., Malmstrom, P.U., Gedda, L., 2005. EGF-receptor targeted liposomes with boronated acridine: Growth inhibition of cultured glioma cells after neutron irradiation. Int. J. Radiat. Biol. 81, 621-629.

Lai, J., Lu, Y., Yin, Z., Hu, F., Wu, W., 2010. Pharmacokinetics and enhanced oral bioavailability in Beagle dogs of cyclosporine A encapsulated in glyceryl monooleate/poloxamer 407 cubic nanoparticles. Int. J. Nanomed. 5, 13−23.

Langston, M.V., Ramprasad, M.P., Kararli, T.T., Galluppi, G.R., Katre, N.V., 2003. Modulation of the sustained delivery of myelopoietin (Leridistim) encapsulated in multivesicular liposomes (DepoFoam). J. Control. Release 89, 87-99.

Lesieur, S., Gazeau, F., Luciani, N., Ménager, C., Wilhelm, C., 2011. Multifunctional nanovectors based on magnetic nanoparticles coupled with biological vesicles or synthetic liposomes. J. Mater. Chem. 21, 14387-14393.

Lim, S.B., Banerjee, A., Önyüksel, H., 2012. Improvement of drug safety by the use of lipid-based nanocarriers. J. Control. Release 163, 34-45.

Martin, F.J., Papahadjopoulos, D., 1982. Irreversible coupling of immunoglobulin fragments to preformed vesicles - an improved method for liposome targeting. J. Biol. Chem. 257, 286-288.

Martins, S., Sarmento, B., Ferreira, D.C., Souto, E.B., 2007. Lipid-based colloidal carriers for peptide and protein delivery - liposomes versus lipid nanoparticles. Int. J. Nanomed. 2, 595-607.

Misiūnas, A., Niaura, G., Barauskas, J., Meškys, R., Rutkienė, R., Razumas, V., Nylander, T., 2012. Horse heart cytochrome C entrapped into the hydrated liquid-crystalline phases of phytantriol: X-ray diffraction and Raman spectroscopic characterization. J. Colloid Interface Sci. 378, 232-240.

Mulet, X., Boyd, B.J., Drummond, C.J., 2013. Advances in drug delivery and medical imaging using colloidal lyotropic liquid crystalline dispersions. J. Colloid Interface Sci. 393, 1-20.

Murakami, S., Ono, T., Sakai, S., Ijima, H., Kawakami, K., 2006. Effect of diglucosamine on the entrapment of protein into liposomes. J. Liposome Res. 16, 103-112.

Negrini, R., Mezzenga, R., 2012. Diffusion, molecular separation, and drug delivery from lipid mesophases with tunable water channels. Langmuir 28, 16455−16462.

Nguyen, T.-H., Hanley, T., Porter, C. J.H., Boyd, B.J., 2011. Nanostructured liquid crystalline particles provide long duration sustained-release effect for a poorly water soluble drug after oral administration. J. Control. Release 153, 180−186.

Patton, J.N., Palmer, A.F., 2005. Photopolymerization of bovine hemoglobin entrapped nanoscale hydrogel particles within liposomal reactors for use as an artificial blood substitute. Biomacromolecules 6, 414-424.

Petersen, A.L., Hansen, A.E., Gabizon, A., Andresen, T.L., 2012. Liposome imaging agents in personalized medicine. Adv. Drug. Deliv. Rev. 64, 1417-1435.

Phan, S., Fong, W.-K., Kirby, N., Hanley, T., Boyd, B.J., 2011. Evaluating the link between self-assembled mesophase structure and drug release. Int. J. Pharm. 421, 176– 182.

Plum, S.M., Holaday, J.W., Ruiz, A., Madsen, J.W., Fogler, W.E., Fortier, A.H., 2000. Administration of a liposomal FGF-2 peptide vaccine leads to abrogation of FGF-2-mediated angiogenesis and tumor development. Vaccine 19, 1294-1303.

Puglia, C., 2008. Lipid nanoparticles for prolonged topical delivery: An in vitro and in vivo investigation. Int. J. Pharm. 357, 295−304.

Ramprasad, M., Amini, A., Kararli, T., Katre, N.V., 2003. The sustained granulopoietic effect of progenipoietin encapsulated in multivesicular liposomes. Int. J. Pharm. 261, 93-103.

Rengel, R.G., Barisic, K., Pavelic, Z., Grubisic, T.Z., Cepelak, I., Filipovic-Grcic, J., 2002. High efficiency entrapment of superoxide dismutase into mucoadhesive chitosan-coated liposomes. Eur. J. Pharm. Sci. 15, 441-448.

Rizwan, S. B., Assmus, D., Boehnke, A., Hanley, T., Boyd, B. J., Rades, T., Hook, S., 2011. Preparation of phytantriol cubosomes by solvent precursor dilution for the delivery of protein vaccines. Eur. J. Pharm. Biopharm. 79, 15−22.

Salentinig, S., Yaghmur, A., Guillot, S., Glatter, O., 2008. Preparation of highly concentrated nanostructured dispersions of controlled size. J. Colloid Interface Sci. 326, 211−220.

Svergun, D.I., 1992. Determination of the regularization parameter in indirect-transform methods using perceptual criteria. *J. Appl. Cryst.* 25, 495-503.

Teiji, O.,Tetsuhiro, K., Yoshitaka, O., Yutaka, F., 2005. Hemodilution with liposome-encapsulated low-oxygen-affinity hemoglobin does not attenuate hypothermic cerebral ischemia in rats. J. Artif. Organs 8, 263–269.

Takeuchi, H., Matsui, Y., Yamamoto, H., Kawashima, Y., 2003. Mucoadhesive properties of carbopol or chitosan-coated liposomes and their effectiveness in the oral administration of calcitonin to rats. J. Control. Release 86, 235-242.

Takeuchi, H., Matsui, Y., Sugihara, H., Yamamoto, H., Kawashima, Y., 2005. Effectiveness of submicron-sized, chitosan-coated liposomes in oral administration of peptide drugs. Int. J. Pharm. 303, 160-170.

Thongborisute, J., Tsuruta, A., Kawabata, Y., Takeuchi, H., 2006. The effect of particle structure of chitosan-coated liposomes and type of chitosan on oral delivery of calcitonin. J. Drug Target. 14, 147-154.

Torchilin, V.P., Rammohan, R., Weissig, V., Levchenko, T.S., 2001. TAT peptide on the surface of liposomes affords their efficient intracellular delivery even at low temperature and in the presence of metabolic inhibitors. Proc. Natl. Acad. Sci. USA 98, 8786-8791.

Turner, D. C.; Gruner, S. M., 1992. X-ray diffraction reconstruction of the inverted hexagonal (H_{II}) phase in lipid-water systems. Biochemistry 31, 1340–55.

Visser, C.C., Stevanovic, S., Voorwinden, L.H., van Bloois, L., Gaillard, P.J., Danhof, M., Crommelin, D.J.A., de Boer, A.G., 2005. Targeting liposomes with protein drugs to the blood-brain barrier *in vitro*. Eur. J. Pharm. Sci. 25, 299-305.

Walde, P., Ichikawa, S., 2001. Enzymes inside lipid vesicles: Preparation, reactivity and applications. Biomol. Eng. 18, 143-177.

Wang, T., Upponi, J.R., Torchilin, V.P., 2012. Design of multifunctional non-viral gene vectors to overcome physiological barriers: dilemmas and strategies. Int. J. Pharm. 427, 3–20.

Wei, M., Xu, Y., Zou, Q., Tu, L., Tang, C., Xu, T., Deng, L., Wu, C., 2012. Hepatocellular carcinoma targeting effect of PEGylated liposomes modified with lactoferrin. Eur. J. Pharm. Biopharm. 46, 131-141.

Woerle, G., Drechsler, M., Koch, M.H.J., Siekmann, B., Westesen, K., Bunjes, H., 2007. Influence of composition and preparation parameters on the properties of aqueous monoolein dispersions. Int. J. Pharm. 329, 150−157.

Xi, J.Q., Guo, R., 2007. Interactions between flavonoids and hemoglobin in lecithin liposomes. Int. J. Biol. Macromol. 40, 305-311.

Xu, X., Costa, A., Burgess, D.J., 2012. Protein encapsulation in unilamellar liposomes: high encapsulation efficiency and a novel technique to assess lipid-protein interaction. Pharm. Res. 29, 1919-1931.

Yaghmur, A., Laggner, P., Zhang, S., Rappolt, M., 2007. Tuning curvature and stability of monoolein bilayers by designer lipid-like peptide surfactants. PLOS ONE 2, e479.

Yaghmur, A., Laggner, P., Sartori, B., Rappolt, M., 2008. Calcium triggered L_{α}-H_2 phase transition monitored by combined rapid mixing and time-resolved synchrotron SAXS. PLOS ONE 3, e2072.

Yaghmur, A., Glatter, O., 2009. Characterization and potential applications of nanostructured aqueous dispersions. Adv. Colloid Interface Sci. 147-148, 333-342.

Ye, Q., Asherman, J., Stevenson, M., Brownson, E., Katre, N.V., 2000. DepoFoam (TM) technology: a vehicle for controlled delivery of protein and peptide drugs. J. Control. Release 64, 155-166.

Zhang, N., Ping, Q.N., Huang, G.H., Xu, W.F., 2005. Investigation of lectin-modified insulin liposomes as carriers for oral administration. Int. J. Pharm. 294, 247-259.

Figure captions

Figure 1. Examples of nanoparticulate lipid carriers that may be derived from PEGylated liquid crystalline lipid phases: (a) hexosome, (b) bilamellar vesicle, and (c) spongosome particles.

Figure 2. Small-angle X-ray scattering (SAXS) patterns (a) and cryo-TEM image (b) of a PEGylated nanoparticulate lipid system (MO/EPA/VitE/V_{1000}, 71/17/8/4 mol.%) interacting with the neurotrophic protein BDNF (brain-derived neurotrophic factor) of solution concentration 8 μg/ml. The blue bars indicate the positions of the Bragg reflections (spaced in the ratio 1: √3: √4: √7) of an inverted hexagonal (H_{II}) lattice structure, which is present in both blank (inset) and BDNF-loaded NPs (a). The inset in (b) shows the Fast Fourier transform (FFT) image analysis of the hexosome lipid nanocarrier.

Figure 3. SAXS patterns (a) and cryo-TEM images (b) of a PEGylated nanoparticulate lipid system (MO/EPA/VitE/V_{1000}, 71/17/8/4 mol.%) interacting with the protein α-chymotrypsinogen A with solution concentration 4 mg/ml. The blue bars in (a) indicate the positions of the Bragg reflections of the inverted hexagonal (H_{II}) structure, which vanished upon protein loading. The inset in (b) shows a second representative NP population in the protein-containing sample.

Figure 4. (a) SAXS patterns (orange curve), a pair distance distribution function ρ(r) (blue curve, inset), and quasi-elastic light scattering (QELS) size distribution plot (inset) measured with histone solution. The protein concentration is 4 mg/ml. (b) QELS determination of the particle size distributions in blank lipid NP formulation (MO/EPA/DOPE-PEG_{2000}, 69/28/3 mol.%) (left) and of the lipid formulation with incubated histone H3 (4 mg/ml) (right). The maxima of the histograms correspond to the most abundant average hydrodynamic particle diameters. The error bars are given in green.

Figure 5. SAXS patterns (a) and cryo-TEM image (b) of a PEGylated nanoparticulate lipid system (MO/EPA/DOPE-PEG_{2000}, 69/28/3 mol.%) interacting with the protein histone H3 with solution concentration 4 mg/ml.

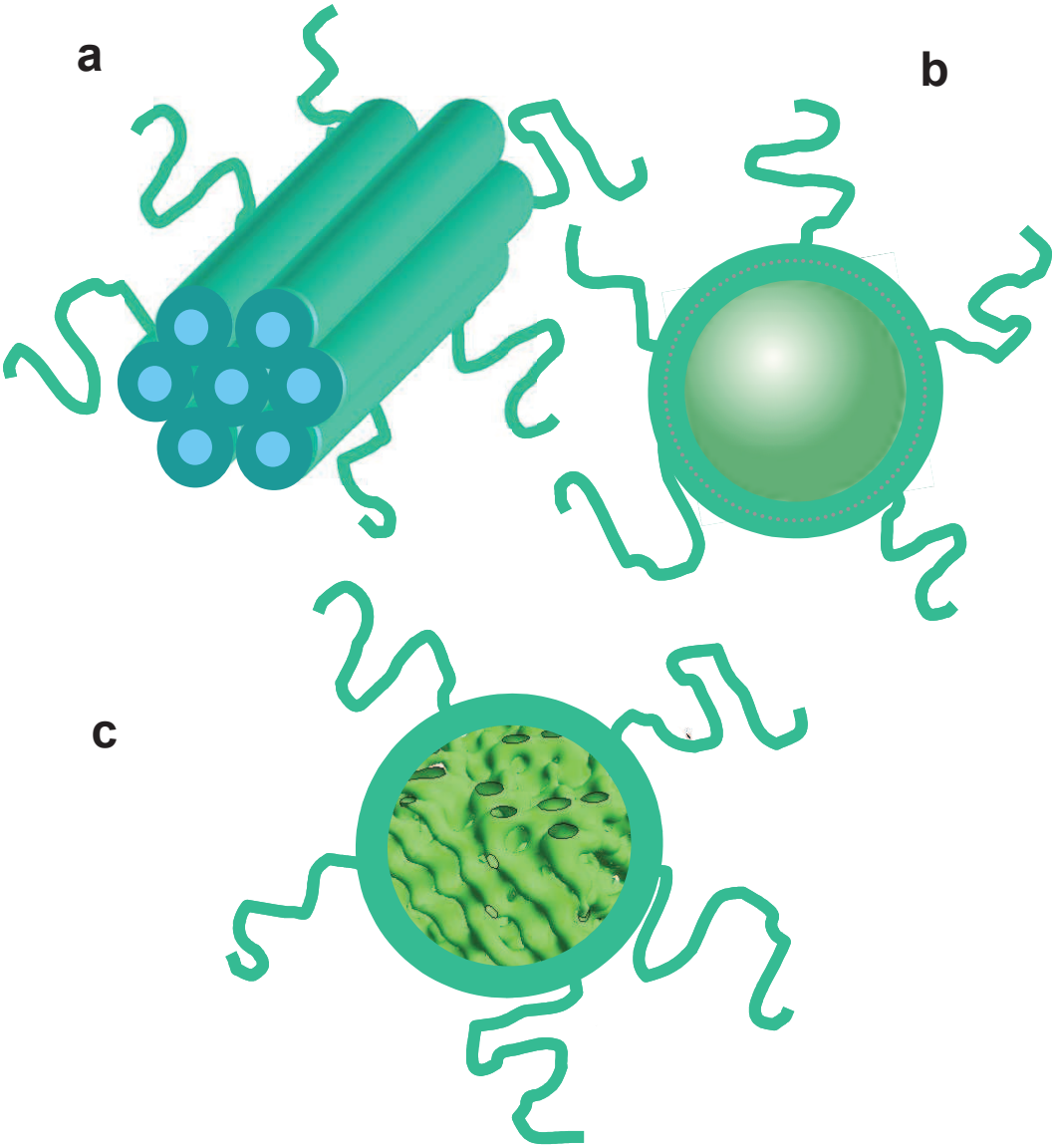

Figure 1

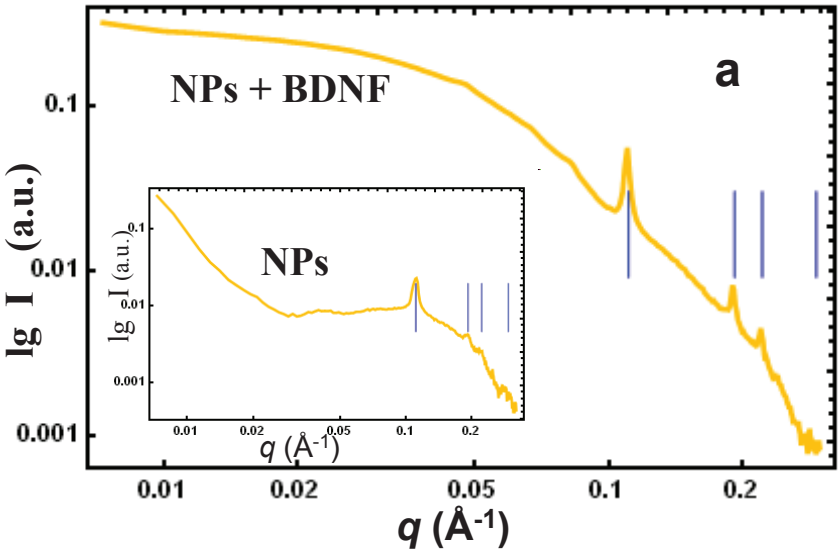
NPs + BDNF
a
NPs
lg I (a.u.)
0.1
0.01
0.001
0.01
0.02
0.05
0.1
0.2
q (Å-1)

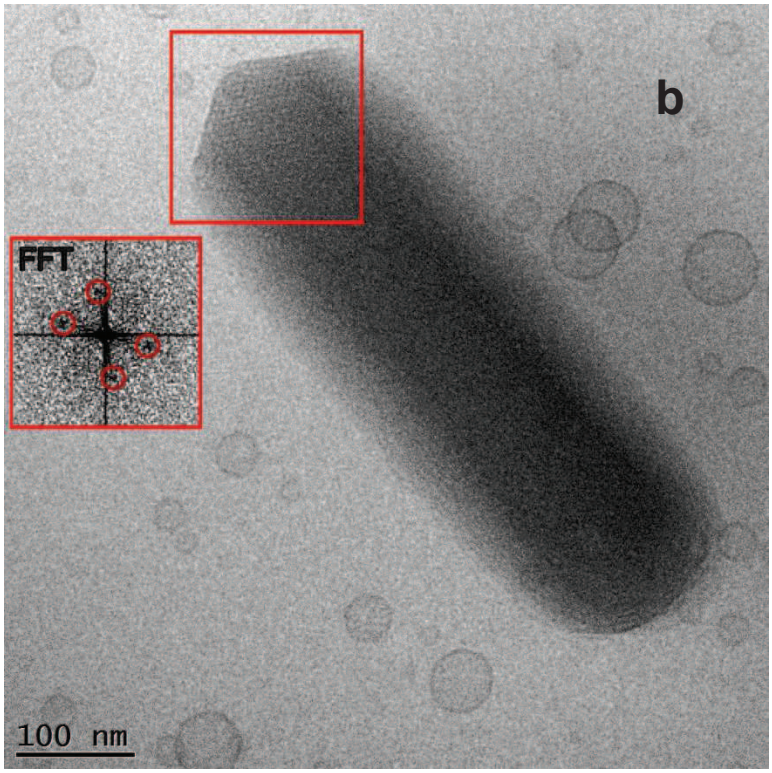
b
FFT
100 nm

Figure 2

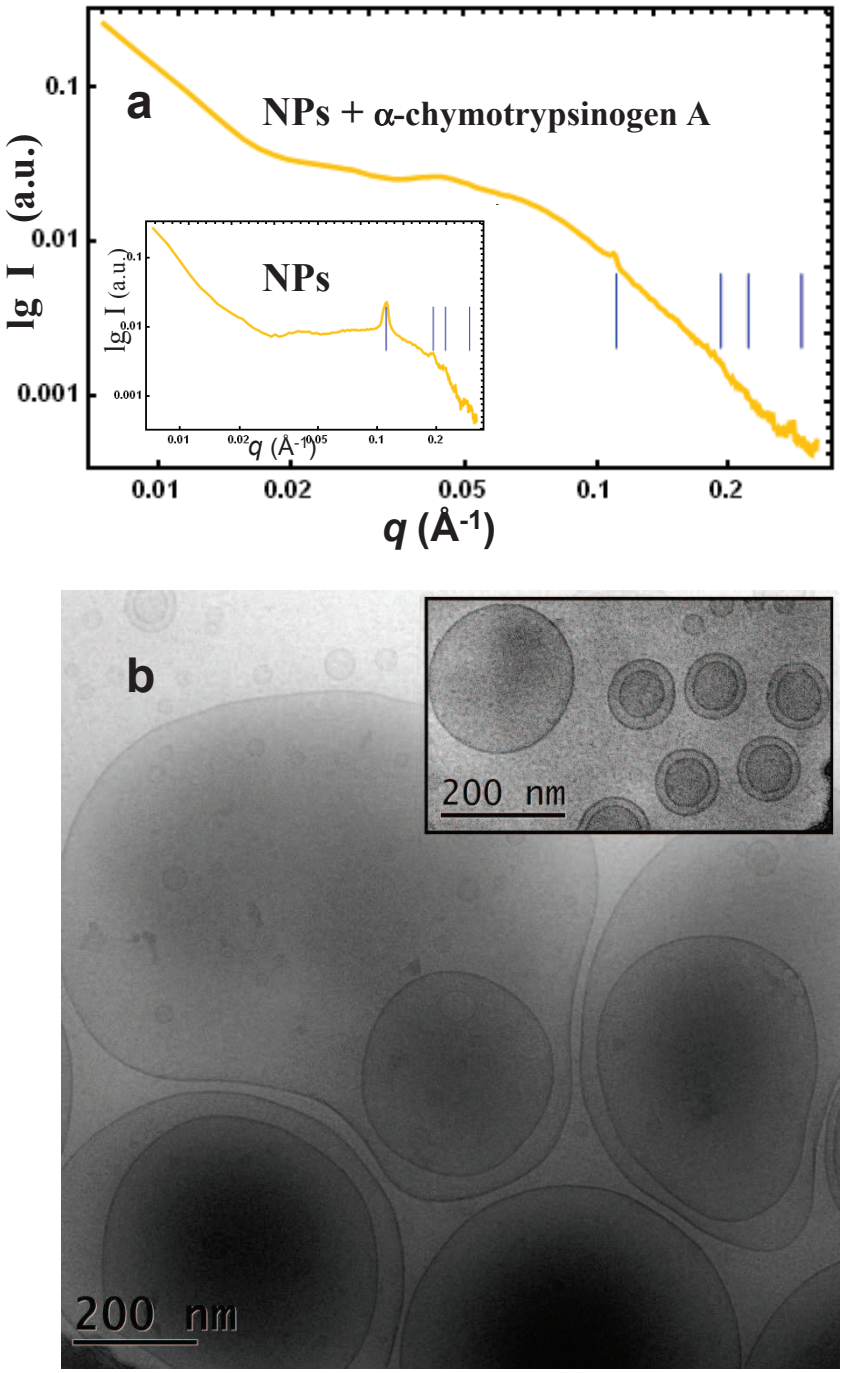
a
NPs + α-chymotrypsinogen A
NPs
lg I (a.u.)
0.1
0.01
0.001
0.01
0.02
0.05
0.1
0.2
q (Å-1)
b
200 nm
200 nm

Figure 3

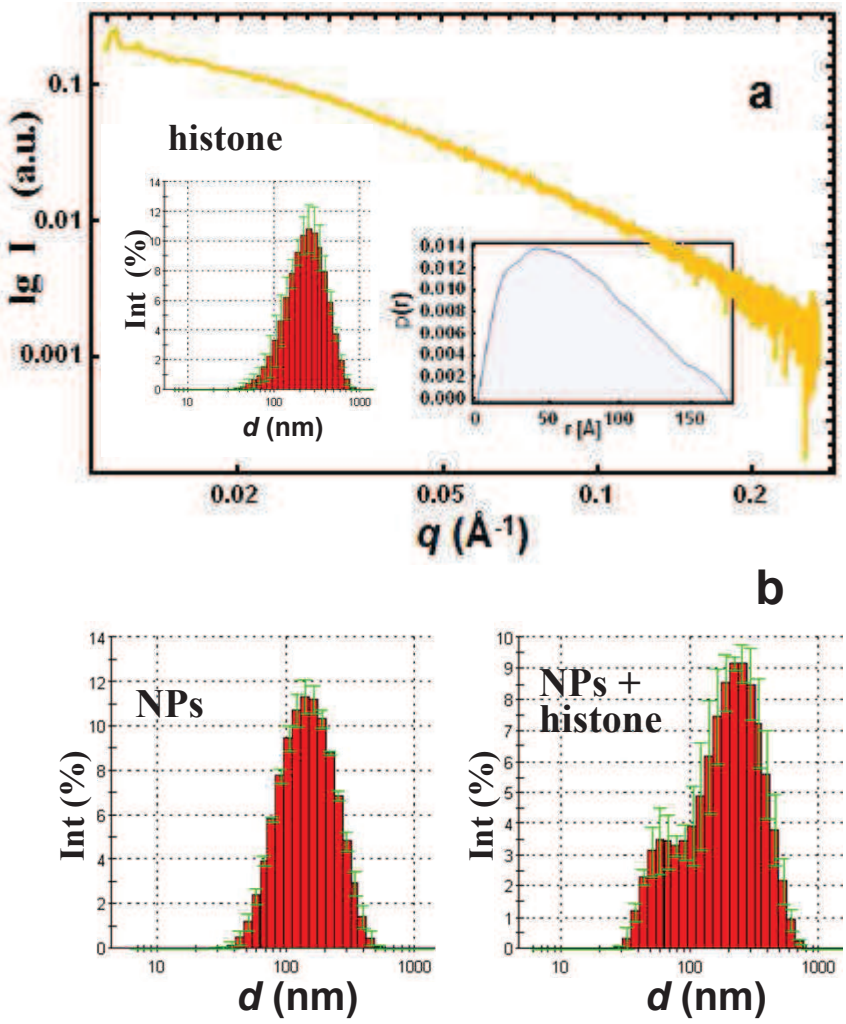
a
histone
lg I (a.u.)
0.1
0.01
0.001
Int (%)
d (nm)
p(r)
r [Å]
0.02
0.05
0.1
0.2
q (Å-1)
b
NPs
NPs +
histone
Int (%)
d (nm)

Figure 4

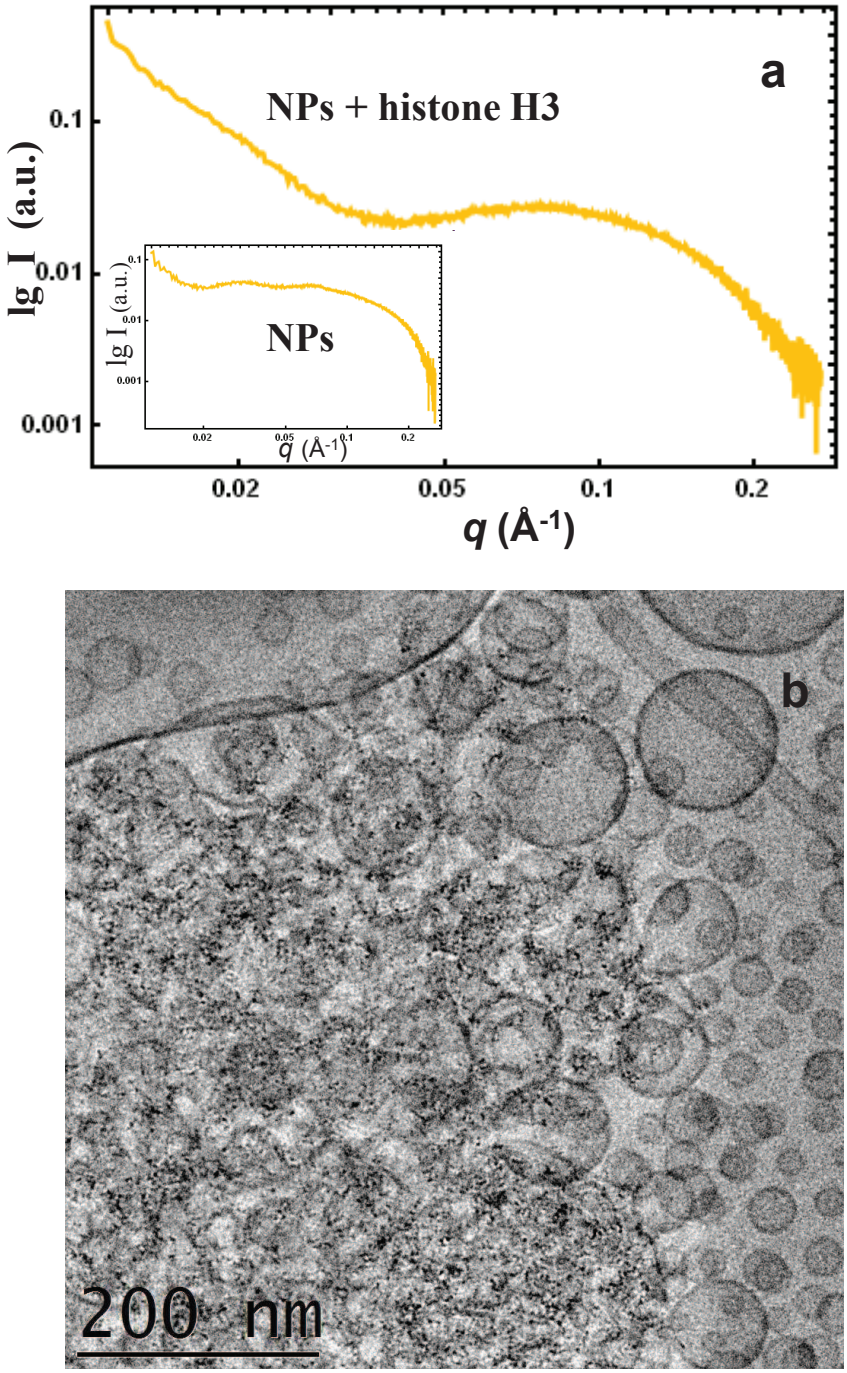

Figure 5

Table 1

Mean particle hydrodynamic diameter, d_h, molecular weight (MW), isoelectric point (pI), and state of protein dissolution/association at the studied concentration in a phosphate buffer aqueous phase. The values of d_h were determined by quasi-elastic light scattering measurements.

Protein	MW [kDa]	pI	concentration	d_h [nm]	state
BDNF	13.6	10.5	8 μg/ml	2.3	dissolved molecules
α-chymotrypsinogen A	25.6	9.2	4 mg/ml	4.8	dissolved molecules
histone	15.3	10.8	4 mg/ml	255	aggregate of 4.5 nm octamers (Fig.4a)